IEEE Access
Multidisciplinary | Rapid Review | Open Access Journal

Received April 18, 2020, accepted April 27, 2020, date of publication May 6, 2020, date of current version May 15, 2020.

Digital Object Identifier 10.1109/ACCESS.2020.2991691

Design, Implementation and Control of a SiC-Based T5MLC Induction Drive System

ABOUBAKR SALEM, (Member, IEEE)
Electrical Engineering Department, King Fahd University of Petroleum and Minerals, Dhahran 31261, Saudi Arabia
e-mail: asalem@kfupm.edu.sa

This work was supported by the Deanship of Research, King Fahd University of Petroleum and Minerals, under Project SR181016.

ABSTRACT This paper presents and evaluate a prototype of an advanced topology of five-level T-type MLC, namely "T5MLC", implemented within a complete AC induction drive. The evaluation is based on the ability of balancing the converter DC link capacitor voltages, the torque and flux ripples reduction of the induction motor under control, the harmonic analysis and the efficiency of the inverter and the overall drive system. The converter implementation and design considerations using Silicon Carbide (SiC) discrete MOSFETs are discussed. The operation and the analytical model of T5MLC using switching-functions are presented. The model predictive control (MPC), as a preferred AC drive control approach, is selected to adapt the machine torque and flux, and to balance the DC link capacitor voltages. The T5MLC drive system is tested at different scenarios; i.e. suddenly load changing and speed reversal, to ensure the converter capability and excellent performance in AC drive applications. The experimental results show that the MPC could achieve an excellent performance in terms of low harmonic distortions, reduced flux and torque ripples and the ability of balanced DC link capacitors. In addition, the loss analysis showed that the T5MLC is 5.5 % to 24.8 % efficient compared to dual T-type MLC at different loading conditions.

INDEX TERMS T-type multilevel converter, model predictive control, capacitor balancing.

NOMENCLATURE

u_s	Stator voltage
i_s	Stator current
ψ_r	Rotor flux
R_s and R_r	Stator and rotor resistances
L_s, L_r and L_m	Stator, rotor, and mutual inductance
$k_r = L_m/L_r$	Rotor coupling facto
ω_r	Electrical rotor speed
$R_\sigma = R_s + k_r^2 R_r$	Equivalent resistance referred to stator
$\tau_r = L_r/R_r$	Rotor time-constan
$L_\sigma = L_s\,(1 - L_m^2/L_r)$	Machine transient inductance
$\tau_\sigma = L_\sigma/R_\sigma$	Stator transient time constant
T	Electrical torqu
n_p	Number of pole pairs
ψ_s	Stator flux.

I. INTRODUCTION

Recently, Diode-Clamped Multilevel Converter (DCMLC) has been enhanced in terms of lower number of semiconductor devices; the matter that reduces the converter cost [1]. One of the enhanced DCMLC is known as T-type MLC. The three-level (3L) and five-level (5L) T-type topologies, have been evaluated compared to the conventional DCMLC in [2], [3] and a better performance has been observed. Modified topologies based on the 3L T-type MLC have been introduced in [4]–[7] to produce 11-, 13-, 15-level and higher voltage levels topologies. These topologies are made in fixable configuration to be extended to higher voltage levels easily for single-phase circuit. However, the extension of these topologies to three-phase circuit will lead to large number of switches and extra separated DC sources for each phase. Recently, a theoretical study for a modified circuit for T-type converter, named T5MLC, has been introduced in [8], [9]. The inverter efficiency has been evaluated compared to the conventional 5L DCMLC and a good performance is observed. However, experimental validation for this has not been introduced yet.

Recently, Silicon Carbide (SiC) MOSFET is chosen in electrical drives converters due to its fast response and lower on- and off-transitions compared to conventional silicon semiconductor technologies [10]. Nevertheless, this fast response SiC semiconductors makes ringing and spikes in the generated voltages in power circuits and printed circuit boards (PCBs). This electromagnetic interference (EMI) issue can be solved by design a prober gate driver circuit and

The associate editor coordinating the review of this manuscript and approving it for publication was Zhixiang Zou.

avoid high stray inductance in the PCB design [11]. Hence, SiC MOSFETs technology use, in particular for advanced MLC topologies, needs quit deep investigations [12]–[14].

Frankly speaking, MLCs need capacitor balancing technique for the DC link. A solution is presented in [15] for the capacitor balancing using external hardware circuit, based on passive elements, which increases the converter complexity, size and cost. In addition, the added passive components are expected to increase the overall converter losses and reduce its efficiency. A better solution for capacitor balancing is to use the converter pulse width modulation (PWM) techniques to balance the DC link as presented in [16]–[19]. The capacitor balancing of T-type MLC has been executed using space vector PWM (SVPWM) in [20]–[22]. However, the extension of SVPWM to converters with higher number of levels requires bulky computation burden. To the best of the author knowledge, no extensive study and practical implementation for capacitor balancing of T5MLC has been conducted, and therefore, this point will be considered in this paper work.

Among of the advanced control techniques, Model Predictive Control (MPC) achieved substantially good performance in electrical drives thanks to the power-electronic converter control discrete nature and the developed technologies in digital controller [23]–[25]. The principle of the MPC approach is to evaluate the drive system model at all of the possible switching states using a cost-function. The switching state that achieve the cost-function optimum solution is used for the next control sample. FCS-MPC technique is preferred in induction drives due to the substantial reduction in torque and flux ripples compared to other control techniques i.e. field oriented control and direct torque control [26]. In addition, MPC technique can control the DC link voltage, reduce the harmonic contents and reduce converter losses in MLCs [27], [28].

In view of the discussions ahead, this paper aims to create a laboratory prototype for T5MLC based on SiC technology and evaluate its performance using FCS-MPC. The assessment of the proposed drive system is measured with regard to flux and torque ripples, capacitor voltage imbalance, the harmonic distortions and the converter as well as the overall drive system efficiency. Therefore, the main contributions of this study are summarized as follows:

- Design, implement and evaluate a SiC-based T5MLC.
- Achieve the capacitor balancing of the T5MLC drives using MPC.
- Evaluate the drive system performance in terms of flux and torque ripples, harmonic distortions, efficiency analysis and ability of the MPC approach to balance the capacitor voltages.

The reminder of this article is structured in the following arrangement. Firstly, the T5MLC operation and analytical model are presented in section II. The MPC of the proposed drive system is presented in Section III. Afterwards, a demonstration of the experimental platform for the T5MLC is described in Section IV. In Section V, the experimental results for the proposed work is discussed and analyzed. A loss analysis and a comparison with the dual T-type MLC is presented and discussed in Section VI. Finally, in Section VII, the work conclusions are derived.

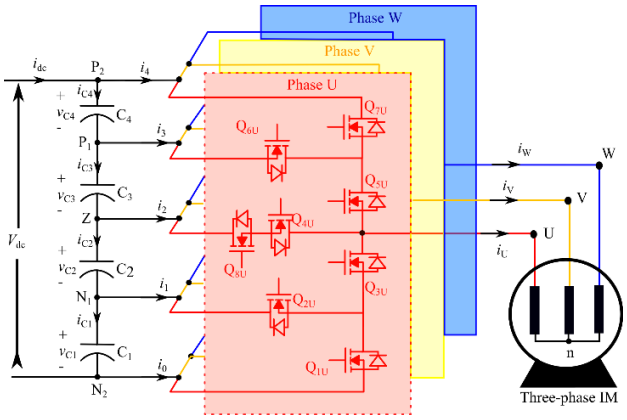

FIGURE 1. Wiring diagram of the three-phase circuit of T5MLC.

TABLE 1. Switching-Function for different mode of operation for phase-U.

Mode		m_U^{P2}	m_U^{P1}	m_U^{Z}	m_U^{N1}	m_U^{N2}	Node	V_{UZ}
S_{5U}, S_{7U}, S_{4U}	→	1	0	0	0	0	P_2	V_{dc}
D_{5U}, D_{7U}, S_{4U}	←							
S_{5U}, D_{6U}, S_{4U}	←	0	1	0	0	0	P_1	$\frac{V_{dc}}{2}$
D_{5U}, S_{6U}, S_{4U}	→							
D_{4U}, S_{8U}	←	0	0	1	0	0	Z	0
S_{4U}, D_{8U}	→							
S_{2U}, D_{3U}, S_{8U}	→	0	0	0	1	0	N_1	$-\frac{V_{dc}}{2}$
D_{2U}, S_{3U}, S_{8U}	←							
D_{1U}, D_{3U}, S_{8U}	→	0	0	0	0	1	N_2	$-V_{dc}$
S_{1U}, S_{3U}, S_{8U}	←							

II. OPERATION AND ANALYTICAL MODEL OF T5MLC

The circuit diagram for a three-phase T5MLC is shown in Fig. 1. Each phase consists of eight semiconductor switches, i.e. (Q_{1X} to Q_{8X}; X is U, V or W). The operation of phase-U of the T5MLC is listed in Table 1 and described in Fig. 2. This figure shows the bidirectional current flow for each operating mode. It is worth mentioning that only one bidirectional switch is needed to implement the T5MLC, which is represented by two anti-series switches Q_{4X} and Q_{8X}. In addition, the switching devices Q_{4U} and Q_{8U} are turned on in different DC-link levels to reduce the switching losses as described in details in [29].

In order to analyze the power electronic converters, a mathematical representation for function of the switching states (SS) is used, namely switching model [30]. Assume m_X^N is the switching function to connect phase X (U, V or W) to node N (P_2, P_1, Z, N_1 or N_2). This function is set to 1 or 0 as clarified in Table 1. The inverter pole-voltages can be described by

$$v_{XZ} = \frac{1}{4}V_{\rm dc}\left(m_X^{\rm P1} - m_X^{\rm N1}\right) + \frac{1}{2}V_{\rm dc}\left(m_X^{\rm P2} - m_X^{\rm N2}\right) \quad (1)$$

Applying KVL for the three-phases, hence,

$$v_{\rm Xn} = v_{\rm XZ} - v_{\rm nZ} \quad (2)$$

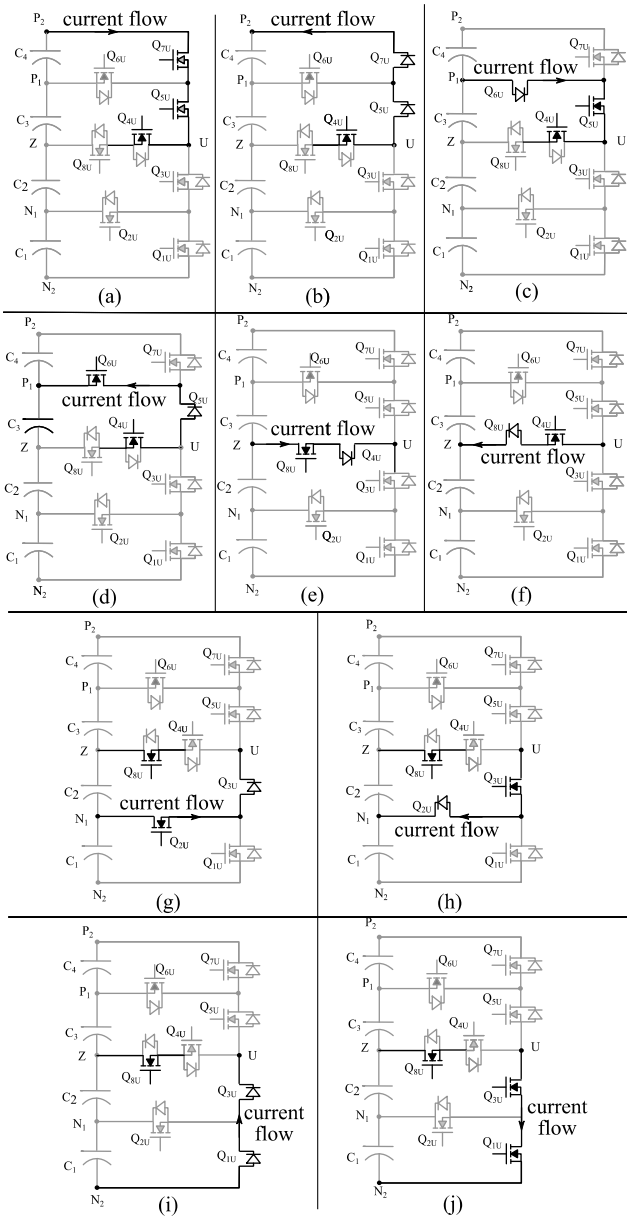

FIGURE 2. Different modes of operation of T5MLC. Bidirectional current flow between (a), (b) P_2 and U, (c), (d) P_1 and U, (e), (f) Z and U, (g), (h) N_1 and U and (i), (j) N_2 and U.

By summing the three voltages $v_{\mathrm{Un}}, v_{\mathrm{Vn}}$ and v_{Wn} of (2), and considering a balanced three-phase voltages, the common-mode voltage v_{nZ} can be described by:

$$v_{\mathrm{nZ}} = \frac{1}{3}\left(v_{\mathrm{UZ}} + v_{\mathrm{VZ}} + v_{\mathrm{WZ}}\right) \tag{3}$$

Using (1), (2) and (3), the voltage v_{Un} can be expressed as:

$$v_{\mathrm{Un}} = \frac{V_{dc}}{12}\Big(2m_{\mathrm{U}}^{\mathrm{P1}} - 2m_{\mathrm{U}}^{\mathrm{N1}} + 4m_{\mathrm{U}}^{\mathrm{P2}} - 4m_{\mathrm{U}}^{\mathrm{N2}} - m_{\mathrm{V}}^{\mathrm{P1}} + m_{\mathrm{V}}^{\mathrm{N1}} - 2m_{\mathrm{V}}^{\mathrm{P2}} + 2m_{\mathrm{V}}^{\mathrm{N2}} - m_{\mathrm{W}}^{\mathrm{P1}} + 2m_{\mathrm{W}}^{\mathrm{N1}} - 2m_{\mathrm{W}}^{\mathrm{P2}} + 2m_{\mathrm{W}}^{\mathrm{N2}}\Big) \tag{4}$$

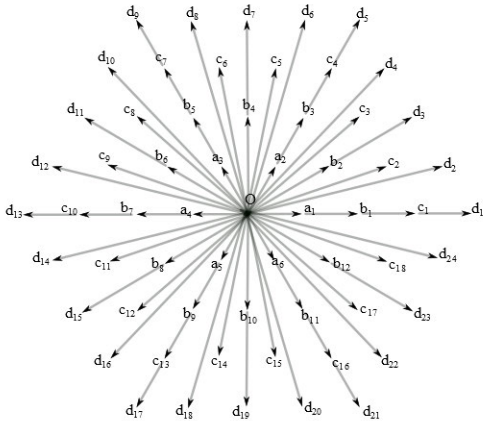

FIGURE 3. Voltage vectors of T5MLC [31].

Similarly, the other two phases can be driven. Applying the switching states probabilities in (4), it could be observed that the phase voltage includes 17 different voltage steps, similar to that of 5LDCC. This topology can attain the vector diagram shown in Fig. 3 that contains 61 voltage vectors that could be achieved using 125 switching states.

The converter current model is required to achieve the capacitor balancing using MPC. The currents $i_0 : i_4$ (See Fig. 1) can be expressed as a function of the three-phase currents and switching-functions as:

$$\begin{aligned} i_4 &= m_{\mathrm{U}}^{\mathrm{P2}} i_{\mathrm{U}} + m_{\mathrm{V}}^{\mathrm{P2}} i_{\mathrm{V}} + m_{\mathrm{W}}^{\mathrm{P2}} i_{\mathrm{W}} \\ i_3 &= m_{\mathrm{U}}^{\mathrm{P1}} i_{\mathrm{U}} + m_{\mathrm{V}}^{\mathrm{P1}} i_{\mathrm{V}} + m_{\mathrm{W}}^{\mathrm{P1}} i_{\mathrm{W}} \\ i_2 &= m_{\mathrm{U}}^{\mathrm{Z}} i_{\mathrm{U}} + m_{\mathrm{V}}^{\mathrm{Z}} i_{\mathrm{V}} + m_{\mathrm{W}}^{\mathrm{Z}} i_{\mathrm{W}} \\ i_1 &= m_{\mathrm{U}}^{\mathrm{N1}} i_{\mathrm{U}} + m_{\mathrm{V}}^{\mathrm{N1}} i_{\mathrm{V}} + m_{\mathrm{W}}^{\mathrm{N1}} i_{\mathrm{W}} \\ i_0 &= m_{\mathrm{U}}^{\mathrm{N2}} i_{\mathrm{U}} + m_{\mathrm{V}}^{\mathrm{N2}} i_{\mathrm{V}} + m_{\mathrm{W}}^{\mathrm{N2}} i_{\mathrm{W}} \end{aligned} \tag{5}$$

III. MODEL PREDICTIVE CONTROL T5MLC IM DRIVE

A schematic diagram for the MPC approach is shown in Fig. 4. The reference speed is compared to the measured one and applied to a proportional-integral controller to generate the torque command. While the flux reference is set to the rated flux value. The induction motor state-space model is used to predict the upcoming flux and torque using the estimated and measured quantities. Then, the cost function is evaluated for the whole number of converter switching state in order to identify the optimum solution. Finally, the switching pattern for the optimum switching state is generated to drive the SiC MOSFETs. In the following subsections, the analytical models for the whole drive system will be described.

A. INDUCTION MACHINE

The stator reference frame induction machine dynamic model considering stator current and rotor flux as the state variables,

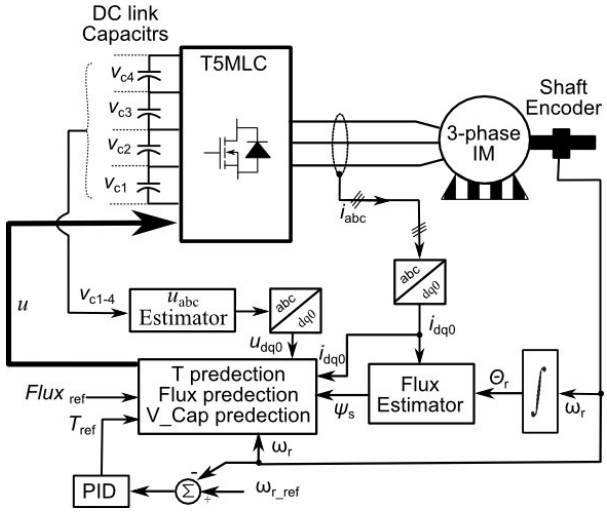

FIGURE 4. Schematic diagram of predictive torque control.

is expressed as follow [32], [33]:

$$\dot{x} = Ax + Bu; \quad \text{where:}$$

$$A = \begin{bmatrix} \frac{-1}{\tau_\sigma} & 0 & \frac{k_r}{R_\sigma \tau_\sigma \tau_r} & \frac{k_r}{R_\sigma \tau_\sigma}\omega_r \\ 0 & \frac{-1}{\tau_\sigma} & -\frac{k_r}{R_\sigma \tau_\sigma}\omega_r & \frac{k_r}{R_\sigma \tau_\sigma \tau_r} \\ \frac{L_m}{\tau_r} & 0 & \frac{-1}{\tau_r} & -\omega_r \\ 0 & \frac{L_m}{\tau_r} & \omega_r & \frac{-1}{\tau_r} \end{bmatrix}, \quad \text{and}$$

$$B = \begin{bmatrix} \frac{1}{R_\sigma \tau_\sigma} & 0 \\ 0 & \frac{1}{R_\sigma \tau_\sigma} \\ 0 & 0 \\ 0 & 0 \end{bmatrix} \tag{6}$$

The machine parameters are defined in the Nomenclature section. The machine electrical torque can be represented by:

$$T = 3/2 n_p(\psi_s \times i_s) \tag{7}$$

In order to predict the torque and flux, the discrete model of induction machine is needed. Several discretization methods can be used as described in [15]. In this work, Euler discretization is preferred for its simplicity. Therefore, discrete state space induction machine model can be described by:

$$\begin{aligned} x^{k+1} &= A_d x^k + B_d u^k \\ A_d &= I + T_s A \\ B_d &= T_s B \end{aligned} \tag{8}$$

where T_s and I represent the sampling time and the identity matrix, respectively.

B. T5MLC MODELLING

Based on the defined switching-function model, the load phase voltage can be calculated by (9)

$$u_s = u_{s\alpha\beta} = V_{dc} T_{Cl} S_{UVW} \tag{9}$$

where V_{dc} is the DC link voltage, S_{UVW} is the T5MLC switching function and T_{Cl} is Clarke transformation that is defined by (10) [32],

$$T_{Cl} = \frac{2}{3}\begin{bmatrix} 0 & -\frac{\sqrt{3}}{2} & \frac{\sqrt{3}}{2} \\ 1 & -\frac{1}{2} & -\frac{1}{2} \end{bmatrix} \tag{10}$$

On the other hand, the rotor flux can be expressed as:

$$\psi_r + \tau_r d\psi_r/dt = L_m i_s \tag{11}$$

and after discretization the rotor flux can be calculated by:

$$\psi_r^k = \frac{L_r}{L_r + T_s R_r}\psi_r^{k-1} + \frac{L_m T_s R_r}{L_r + T_s R_r} i_s^k \tag{12}$$

C. FLUX AND TORQUE PREDICTION

By means of stator current and rotor flux, the stator flux can be predicted one step ahead using:

$$\psi_s^{k+1} = k_r \psi_r^{k+1} + L_\sigma i_s^{k+1} \tag{13}$$

It is worth mentioning that state variables in (8) and (13) are expressed in stator reference frame. Hence, rotor to stator transformation has to be used firstly.

Frankly speaking, calculations are time consuming. Therefore, one step ahead may be not sufficient to be applied in time. Therefore, a prediction at sample $k+2$ is calculated as follows:

$$\begin{aligned} x^{k+2} &= A_d x^{k+1} + B_d u^{k+1} \\ \psi_s^{k+2} &= k_r \psi_r^{k+2} + L_\sigma i_s^{k+2} \\ T^{k+2} &= \frac{3}{2} n_p(\psi_s^{k+2} \times i_s^{k+2}) \end{aligned} \tag{14}$$

D. CAPACITOR VOLTAGE BALANCING

The reason behind the capacitor unbalance of T5MLC is the unequal current sharing of the four capacitors [29]. The solution of such problem is implemented in [15] using external hardware, which increases the converter complexity and losses.

The proposed solution in this paper is software solution-based. Frankly speaking, the redundant switching state for the same voltage vector have different effects on the capacitor charging case. Therefore, the capacitor balancing for different MLC is considered switching state dependent [31]. In order that, the proposed work is based on using MPC technique to balance the DC link capacitors.

For a capacitor, x:

$$dv_{Cx}/dt = i_{cx}/C_x \tag{15}$$

Using Euler discretization, the predicted capacitor voltage can be expressed as

$$v_{Cx}^{K+1} = v_{Cx}^K + i_{Cx}^{K+1}.T_s/C_x \tag{16}$$

The capacitor currents can be expressed as a function of the $i_0 : i_4$ as follows:

$$\begin{aligned} i_{C4} &= i_{dc} - i_4 \\ i_{C3} &= i_{dc} - i_4 - i_3 \\ i_{C2} &= i_{dc} - i_4 - i_3 - i_2 \\ i_{C1} &= i_{dc} - i_4 - i_3 - i_2 - i_1 \end{aligned} \tag{17}$$

The current $i_0 : i_4$ can be obtained as a function of the three-phase currents and switching as described by (5). In order to achieve capacitor balancing, each capacitor has to share the same amount of energy. Therefore, $i_{dc} = 0$ [34]. So, $i_{C1} : i_{C4}$ can be expressed as

$$\begin{aligned} i_{C4} &= -i_4 \\ i_{C3} &= -i_4 - i_3 \\ i_{C2} &= -i_4 - i_3 - i_2 \\ i_{C1} &= -i_4 - i_3 - i_2 - i_1 \end{aligned} \tag{18}$$

E. MPC COST-FUNCTION

The target of the MPC here is to apply the capacitor balancing and control the machine torque and flux. Therefore, the cost-function includes flux, torque, and capacitor voltage deviations as:

$$J = K_{dc}\left[\sum_{x=1}^{3}\left(v_{Cx}^{k+2} - v_{C(x+1)}^{k+2}\right) + \left(v_{C1}^{k+2} - v_{C4}^{k+2}\right)\right] + \frac{\left|T^{ref} - T^{k+2}\right|}{T_{rated}} + K_{\psi}\frac{\left|\left\|\psi_s^{ref}\right\| - \left\|\psi_s^{k+2}\right\|\right|}{\|\psi_s\|_{rated}} \tag{19}$$

where T^{ref} and ψ_s^{ref} are the desired torque and flux respectively. T_{rated} is the rated torque and $\|\psi_{rated}\|$ is the rated stator flux magnitude. K_{ψ}, K_{dc} are the flux and the capacitor voltage weighting factors. These factors determine the relative importance of flux, capacitor voltages errors. During design process, these factors should be carefully tuned in order to get an acceptable performance. A flow-chart T5MLC MPC approach is described in Fig. 5.

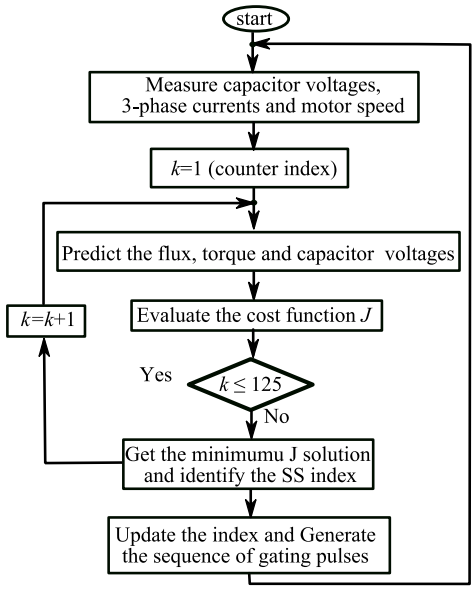

FIGURE 5. T5MLC MPC approach flowchart.

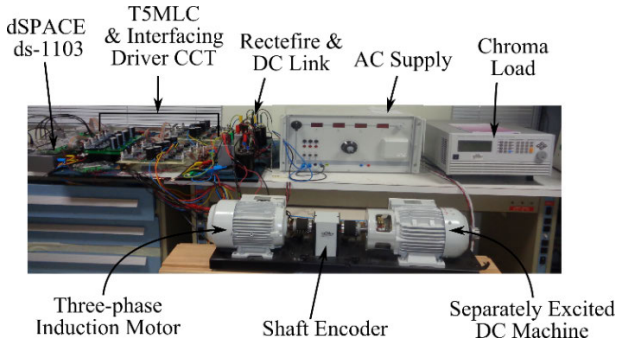

FIGURE 6. Prototype of the T5MLC connected to dS1103 and interfacing circuits.

IV. EXPERIMENTAL PROTOTYPE OF T5MLC DRIVE SYSTEM

The Silicon Carbide (SiC) semiconductor technology is preferred compared to conventional Silicon IGBTs as well as Si MOSFETs thanks to the lower transition periods that substantially affect the converter performance and decreases the switching losses. This loss reduction and fast response are due to the lower turn-on and off periods of the SiC MOSFETS compared to that of Silicon based devices [36]. However, the fast response of the SiC MOSFET causes ringing.

On the other hand, for MLCs PCBs, the high number of switching devices per circuit requires many long traces to connect between switching devices and to interface their driver circuits. This leads to increase the stray inductance and may cause EMI issues [13]–[16]. Therefore, developers produced T-type modules for only one-phase to avoid EMI problems [35]. Similarly, the proposed converter is implemented based on designing each phase at a separate PCB. This allows to keep short traces between power switches to reduce the traces length and their stray inductance. In addition, the traces between the semiconductor switches and drivers are kept small as possible to avoid ringing effect on the inverter AC side. In addition, DC link capacitors are also placed on the same PCB and close to the semiconductor switches to prevent ringing and high stray inductance values. The prototype of the implemented converter is shown in Fig. 6. The T5MLC prototype is implemented using SiC discrete MOSFETs (Model # C2M0080120D). The MOSFETs are interfaced to Cree driver circuit (model #: CGD15HB62P1). The drivers are interfaced to dSPACE 1103 digital controller through dead-band circuit that isolates the converter power circuit from the controller and prevent the expected short circuit due switching pulses overlapping.

A schematic diagram for the test platform is shown in Fig. 7. It consists of a T5MLC supplying a three-phase induction motor of the name-plate data given in Appendix A. This motor is supplying a DC machine that is electrically loaded by a programmable load in order to achieve a certain load torque on the induction motor. Twisted ribbon cables

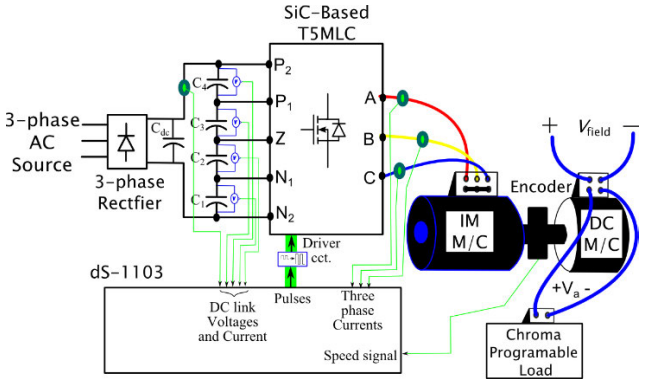

FIGURE 7. Block diagram for the experimental platform.

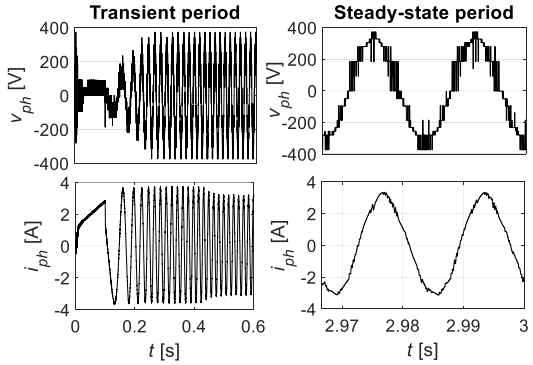

FIGURE 8. Case I- Machine voltage and current at transient and steady state [Simulation].

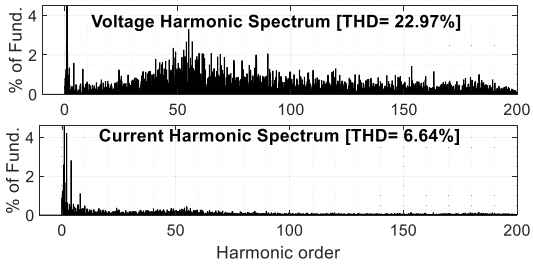

FIGURE 9. Case I- Voltage and current harmonic spectra [Simulation].

are used to interface the gating signals between dSPACE and driver circuits. This type of cables is used in order to avoid the normal wiring noise. The three-phase currents, the four capacitor voltages and the motor speed are measured and interfaced to dS-1103 digital controller.

V. RESULTS AND DISCUSSIONS

To evaluate the proposed drive system, the following scenarios are performed:

- Case I (Ignoring Capacitor Balancing): in which the drive system will be tested while neglecting the capacitor balancing. This test aims to reflect the drive system performance if the capacitors are not balanced. It will be implemented using $K_{dc} = 0$.
- Case II (Suddenly Load Changing): in which the capacitor balancing is considered from the starting time. At a certain instant, a suddenly load changing is applied to reflect how the algorithm can restore the operating point and balance the capacitors safely.
- Case III (Reverse Motoring): in which the machine will be started at motoring operation at a certain loading condition. Then the torque and speed commands will be reversed in order to operate the motor at the fourth quadrant (Torque and speed are negative values). This test is implemented experimentally using a resistive load instead of the Chroma programmable load.

It is worth mentioning that the weighting factor tuning is performed using extensive off-line calculations, using the technique described in [37].

To evaluate the drive system properly, the experimental tests have been performed as follows. The flux command is given to the controller 0.1 s before applying the speed command. This allows to fulfill the machine excitation and reduces the starting current. In addition, the Chroma programmable load is controlled from dSPACE to apply the load command at $t = 0.25\ s$.

A. CASE I: TORQUE CONTROL WHILE CAPACITOR BALANCING IS IGNORED

In this mode, the capacitor balancing is ignored by setting weighting factor to zero. The simulation results for this case are shown in Fig. 8, Fig. 9 and Fig. 10, while the corresponding experimental results are shown in Fig. 11, Fig. 12 and Fig. 13. The machine voltage and current at transient and at steady state periods are shown in Fig. 8. The phase voltage waveform steps appeared distorted due to the capacitor voltage unbalance and accordingly, the current seems distorted. In addition, the voltage and current waveforms have been analyzed using Fourier.

The harmonic spectra for phase voltage and current are shown in Fig. 9. The total harmonic distortion (*THD*) values are declared on the same figure. On the other hand, the induction machine speed, torque and flux are recorded and plotted along with the DC link capacitor voltages in Fig. 10. It could be observed that the torque and flux have peak to peak ripples of 0.71 N.m. and 21.9 mWb, respectively. In addition, the maximum capacitor voltage could be observed for capacitor C_1 is 285.5 V.

The experimental results show similar trends in the voltage and current waveforms. The voltage and current waveforms seems distorted due to the capacitor voltages unbalance similar to the recorded simulation results. Moreover, slight difference in *THD* values could observed compared to simulation voltage and current *THD* values. This slight difference results from the accuracy of the current and voltage sensors and the used data acquisition system. Regarding the machine performance, it could be observed that the torque and flux have peak to peak ripples of 1 N.m and 32 mWb, respectively. Although the required voltage for each capacitor is 140 V, capacitor C_1 reached to 300 V due to ignoring the capacitor balancing in this case study.

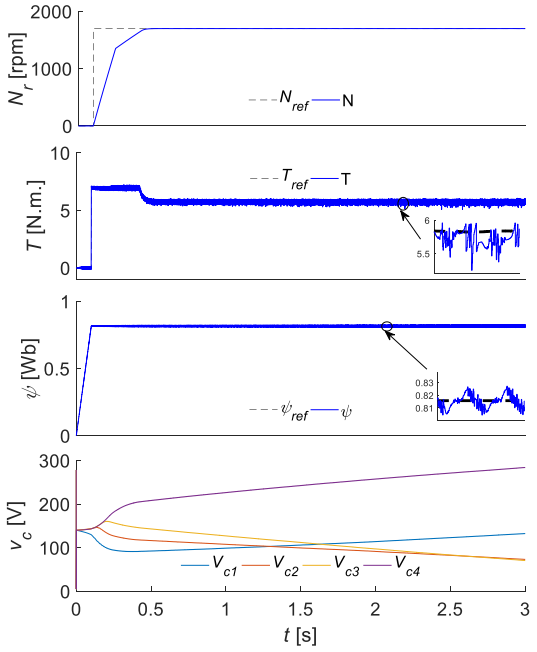

FIGURE 10. Case I- Machine speed, torque ad flux along with DC link capacitor voltages [Simulation].

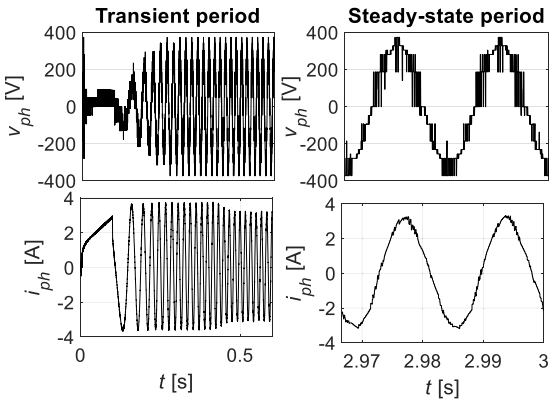

FIGURE 11. Case I- Machine voltage and current at transient and steady state periods [Experimental].

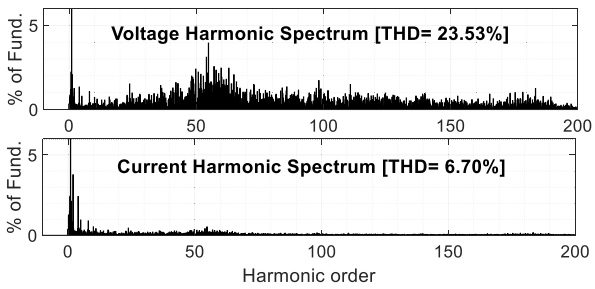

FIGURE 12. Case I- Voltage and current harmonic spectra [Experimental].

Comparing simulation and experimental results, a slight difference in all factors can be observed. The voltage and current *THD* values have slight errors of 2.38% and 0.89%, respectively. Considering the machine rated torque and flux as references, the torque and flux ripples errors have been

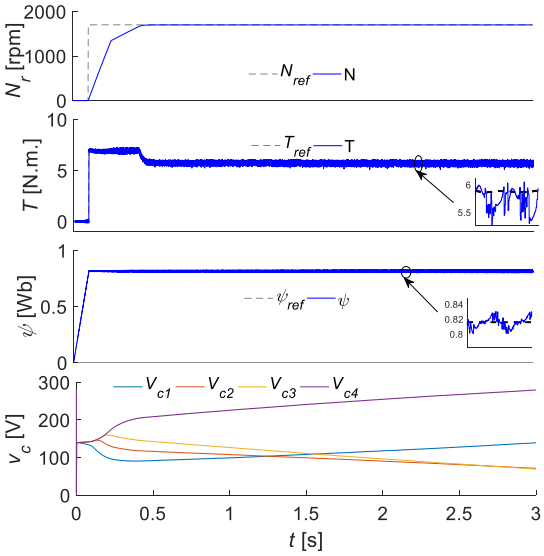

FIGURE 13. Case I- Machine speed, torque ad flux along with DC link capacitor voltages [Experimental].

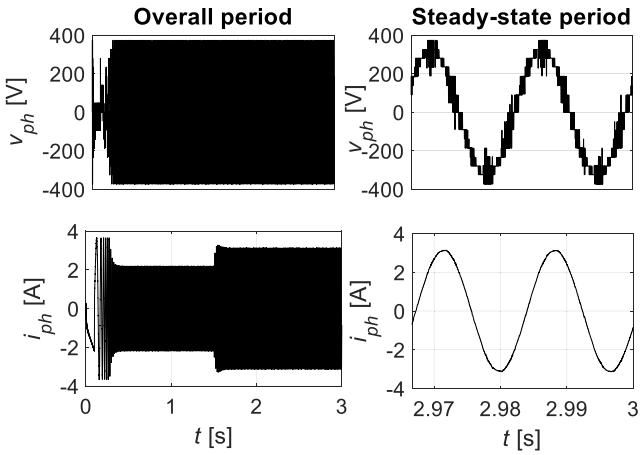

FIGURE 14. Case II- Machine voltage and current at transient and steady state periods [Simulation].

calculated. It could be observed that the torque and flux errors are 5.27% and 1.24%, respectively.

B. CASE II: TORQUE CONTROL WHILE CONSIDERING CAPACITOR BALANCING

In this case, the machine is started while considering the capacitor balancing. Firstly, 2 N.m load is applied at $t = 0.25\ s$. Then, the machine full load (5 N.m) is suddenly applied at $t = 1.5\ s$. The simulation results for Case II are shown in Fig. 14, Fig. 16 and Fig. 17, while the experimental results are shown in Fig. 18, Fig. 19 and Fig. 20. The machine voltage and current overall and at steady state periods are shown in Fig. 14. The overall period is recorded here to observe the load increase. The phase voltage waveform steps appeared different compared to Case I due to the balanced DC link capacitors. However, the waveform still appears distorted and have relatively high harmonic contents compared to classical SVPWM that is shown in Fig. 15. The reason behind

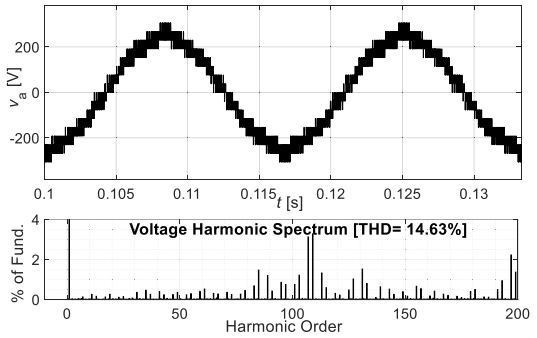

FIGURE 15. Voltage waveform and spectra for T5MLC using SVPWM [Simulation].

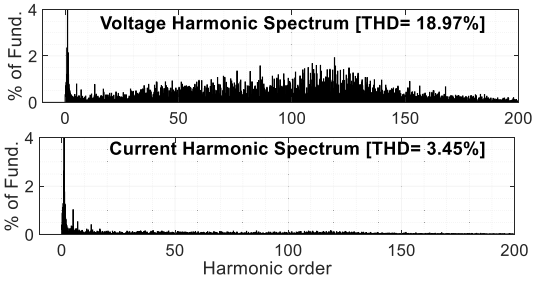

FIGURE 16. Case II- Voltage and current harmonic spectra [Simulation].

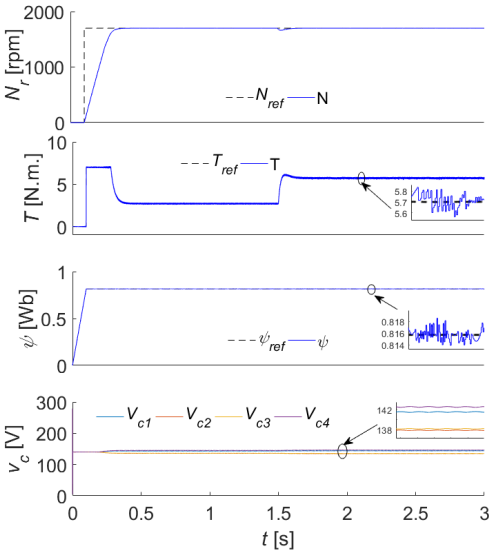

FIGURE 17. Case II- Machine speed, torque ad flux along with DC link capacitor voltages [Simulation].

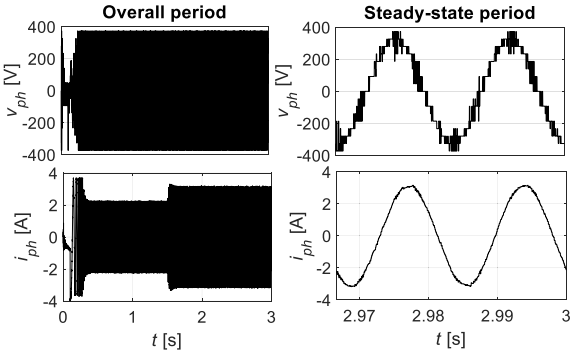

FIGURE 18. Case II- Machine voltage and current at transient and steady state periods [Experimental].

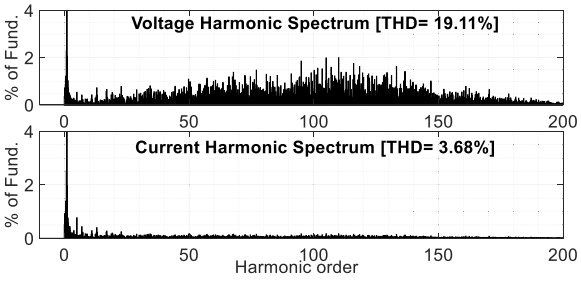

FIGURE 19. Case II- Voltage and current harmonic spectra [Experimental].

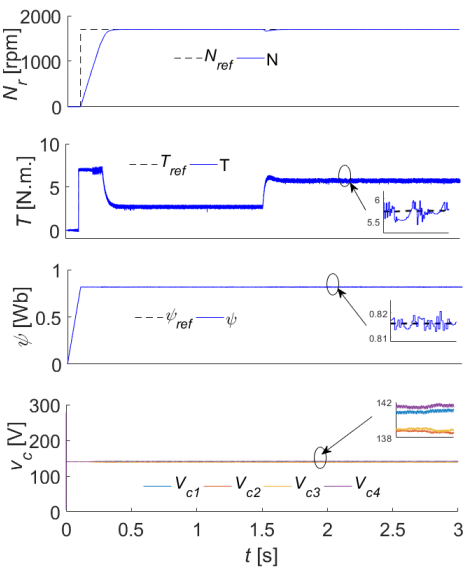

FIGURE 20. Case II- Machine speed, torque ad flux along with DC link capacitor voltages [Experimental].

that is the nature of the MPC that can change the converter switching states only in times of a relatively high sampling time, which is 70μs in case of MPC for T5MLC drives using dS1103 digital controller. Therefore, higher *THD* value and subharmonic contents can be observed in Fig. 16 compared to that of Fig. 15.

On the other hand, the induction machine speed, torque and flux are recorded and plotted along with the DC link capacitor voltages in Fig. 17. It could be observed that the torque and flux have peak to peak ripples of 0.27 N.m. and 4.6 mWb, respectively. In addition, the maximum capacitor voltage could be observed for capacitor C_1 is 143 V. It is worth mentioning that a small dip in the machine speed is appeared at the instance of the suddenly load. In addition, a small deviation is recorded in the capacitor voltages due to that load increase. However, the control technique could achieve the command speed in relatively small period (0.15 s). The experimental results show similar trends in the voltage and current waveforms. Slight difference in *THD* values could observed compared to simulation voltage and

TABLE 2. Comparison between the three case studies.

Cases	Case I		Case II	
	Sim.	Exp.	Sim.	Exp.
$T_{ripples}$ [N.m]	0.71	1.00	0.27	0.51
% $T_{ripples}$ *	12.90	18.18	4.90	9.27
$\varphi_{ripples}$ [mWb]	21.90	32.00	4.60	6.20
% $\varphi_{ripples}$ *	2.68	3.92	0.56	0.76
THD_i [%]	6.64	6.70	3.45	3.68
THD_v [%]	22.97	23.53	18.97	19.11
Max. $\Delta \boldsymbol{V_c}$ [V]	285.50	300.00	143.00	145.00
Max. $\Delta \boldsymbol{V_c}$ [%]	104.00	114.00	2.14	3.57

*: all percent values are referred to desired or rated values.

current *THD* values. Regarding the machine performance, it could be observed that the torque and flux have peak to peak ripples of 0.51 N.m and 6.2 mWb, respectively. The maximum observed capacitor voltage is 145 V. Comparing simulation and experimental results, a slight difference in all factors can be observed. The voltage and current *THD* values have slight errors of 0.73% and 6.25%, respectively. Considering the machine rated torque and flux as references, the torque and flux ripples errors have been calculated. It could be observed that the torque and flux errors are 4.36% and 0.19%, respectively.

Comparing Case II with Case I, a summary for the torque ripples, the flux ripples and the voltage and current *THD* values for both simulation and experimental results are listed in Table 2. The capacitor balancing has positively affect the drive system performance. The torque ripples have been reduced by 8% and 8.9% for simulation and experimental results respectively. In addition, the flux ripples could be reduced by 2.12% and 3.16% for simulation and experimental results, respectively. In addition, the voltage *THD* could be reduced by 21% and 23.13% for simulation and experimental results, respectively. Similarly, the current THD values could be reduced by 92.46% and 82.07% for simulation and experimental results, respectively.

For the DC link capacitor voltages, assume that the absolute capacitor voltage imbalance is calculated by:

$$\Delta V_c\% = |V_{des} - V_{ci}| / V_{des} * 100\% \tag{20}$$

The capacitor voltage imbalance values are listed in the same table. Comparing Case II with Case I, the imbalance ratio could be decreased by 101.86% and 110.43% respectively.

C. CASE III: REVERSE MOTORING

Frankly speaking, reverse motoring test at full load is a well-known technique to measure the drive system performance, where the machine is suddenly forced to reverse its direction and at high value of load torque. Therefore, this test is implemented in this proposed work to measure how the proposed drive system is reliable. This test is carried out while applying a resistive load to the DC generator with similar steady state load torque value to the cases I and II. Firstly, the controller gives the command speed and torque at $t = 0.1$ and $t = 0.25$ s, respectively. Then, at $t = 1.5$ s, commands of negative sign torque and speed commands are

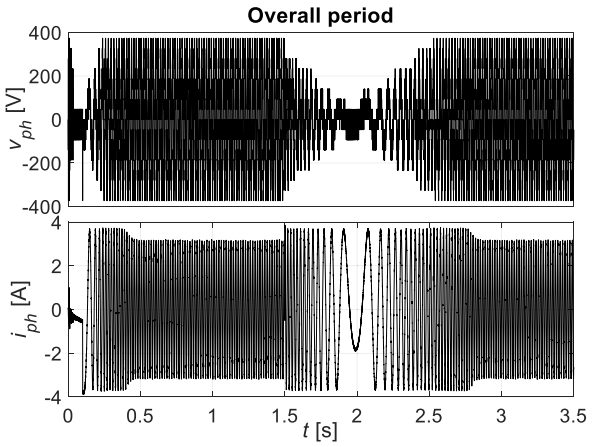

FIGURE 21. Case III- Machine voltage and current [Simulation].

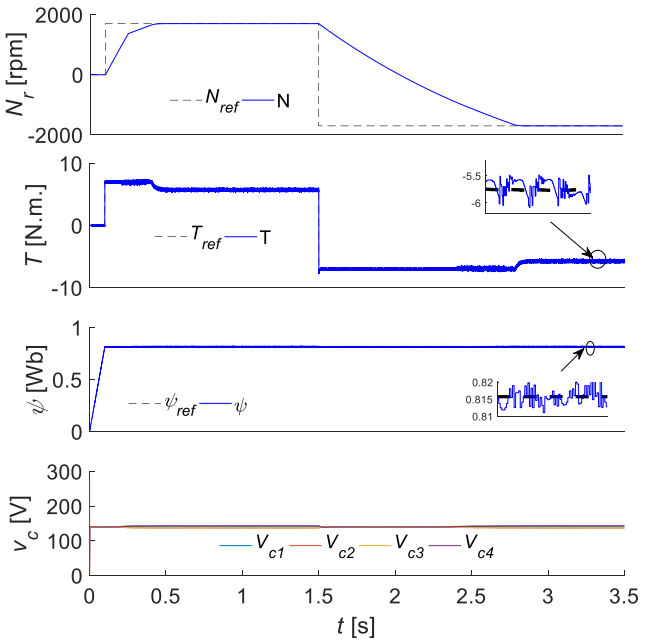

FIGURE 22. Case III- Machine speed, torque ad flux along with DC link capacitor voltages [Simulation].

given to the drive system. The voltage and current responses are shown in Fig. 21 and Fig. 23 for simulation and experimental results, respectively. The machine speed, torque and flux along with the DC link capacitor voltages are shown in Fig. 22 and Fig. 24 for simulation and experimental results, respectively. Both simulation and experimental results are in full agreement. The machine reached to zero speed at $t = 2$ s, and the machine completely reached to steady state reversed speed at $t = 2.8$ s. Therefore, the drive system could reverse the machine in a small time of 1.3 s. The results reflect that the controller could reverse the motor operation safely without any dangerous current or torque spikes.

In addition, the capacitor balancing could be achieved without any voltage dip as seen in the same figure. This reflects how this drive system with its applied control approach are able to work with harsh drive systems conditions.

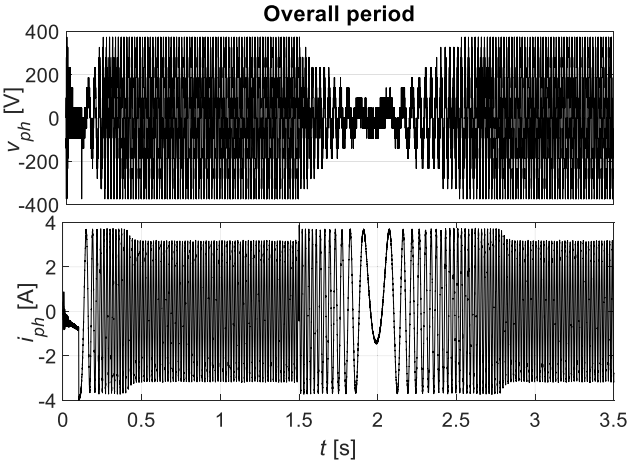

FIGURE 23. Case III- Machine voltage and current for the overall period [Experimental].

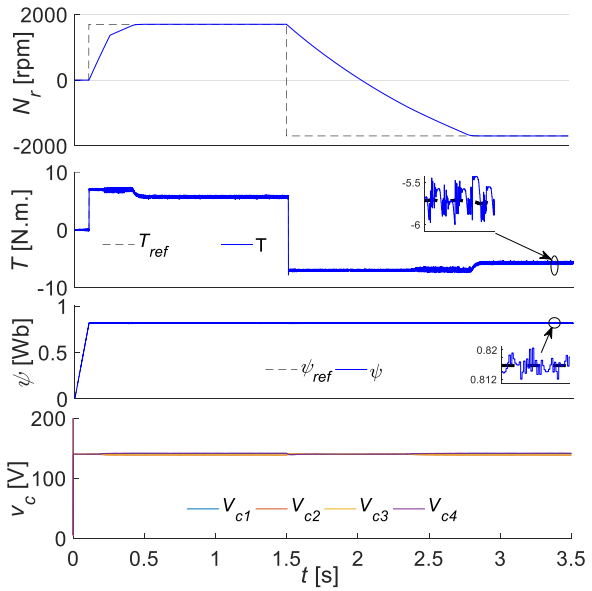

FIGURE 24. Case III- Machine speed, torque ad flux along with DC link capacitor voltages [Experimental].

VI. LOSS EVALUATION OF T5MLC COMPARED TO DUAL T-TYPE MLC

A loss analysis for the T5MLC is made based on recording the input DC voltage and currents, the output AC voltages and currents and the output shaft torque and speed. A comparison is made with the corresponding T-type MLC with similar number of voltage levels, which is dual T-type (DTT) MLC. The IM drive system is loaded by a DC machine and Chroma programmable load in this test. The test aims to evaluate the motor and inverter efficiencies at different loading conditions. The test has been performed while changing the Chroma load drawn current to achieve different values of loading torque. Fig. 26 shows the motor and inverter efficiencies while mechanical load is varying from 0.3 N.m to 5.5 N.m at 1700 RPM speed command. The results show that the T5MLC IM drive system is efficiency is higher than that of DTT system. In addition, the T5MLC efficiency is substantially high compared to that of DTT. For instance, the efficiency of the T5MLC is higher than that of DTT by 24.8 % and 5.5 % at rated load torque values 0.5 N.m and 5.5 N.m, respectively.

To validate the experimental results, the T5MLC loss analysis is performed using the loss model described in [29], [38]. The model is based on calculating the loss for individual switches due to the different switching frequency of each semiconductor used in multilevel converters. Therefore, the power loss is calculated for T5MLC by summing the loss of the converter semiconductor switches as performed. The switching losses are calculated assuming that the energy loss curve is varying linearly with the drain current.

The switching loss is calculated based on the following strategy:

1. Obtaining the semiconductor switch parameters from the datasheet. The MOSFET parameters are the drain to source voltage $V_{\rm ds}$, the MOSFET equivalent resistance during on state $R_{\rm on}$, the turn on and turn off energy losses $E_{\rm on}$ and $E_{\rm off}$, which are given in the datasheet at a reference voltage $V_{\rm ref}$ and a reference current $I_{\rm ref}$. The antiparallel diode parameters are the reverse recovery charge $Q_{\rm rr}$, the equivalent diode resistance during on state $R_{\rm d-on}$, and the diode turn on voltage $V_{\rm d-on}$.
2. Obtaining the number of turning on and off transitions per electrical period.
3. Obtaining the turn-on and the turn-off current values for each switch.

The MOSFET switching loss can then be calculated as follows [29]:

$$\begin{aligned} P_{sw-on} &= \frac{V_{ds}E_{onf}}{V_{ref}I_{ref}}\sum_{k=1}^{k_s} I_{on-k} \\ P_{sw-off} &= \frac{V_{ds}E_{offf}}{V_{ref}I_{ref}}\sum_{k=1}^{k_s} I_{off-k} \\ P_{sw} &= P_{sw-on} + P_{sw-off} \\ P_{d.sw-on} &= \frac{1}{4}Q_{rr}.V_{Drr}.f \end{aligned} \tag{21}$$

where $P_{\rm sw-on}$ is the turn on switching loss, $P_{\rm sw-off}$ is the turn off switching loss, $P_{\rm sw}$ is the total switching losses, $K_{\rm s}$ is the number of pulses per electrical period, f is the frequency of the electrical period (which is 60 Hz in this study), $I_{\rm on}$ is the turn on current and $I_{\rm off}$ is the turn off current. An example to describe the meaning of the summation in (21) for a switch current is shown in Fig. 25. This figure shows a current has $K_{\rm s}$ pulses. At $k = 1$, $\rm I_{on-1}$ is used to calculate the turn on loss, and $\rm I_{off-1}$ is used to calculate the turn off loss. The total switching losses can be described by the summation of the loss of the different pulses ($k = 1$: $K_{\rm s}$). The MOSFET and the diode conduction losses can be calculated as follows [29]:

$$\begin{aligned} P_{\rm cond} &= I^2 R_{\rm on} \\ P_{\rm d-cond} &= I_d^2 R_{\rm d-on} + I_d^{av} V_{\rm d-on} \end{aligned} \tag{22}$$

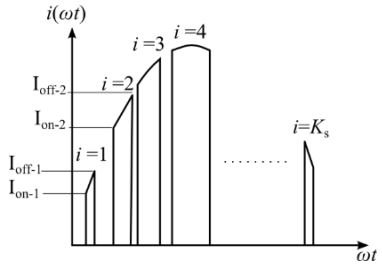

FIGURE 25. Example for one switch current.

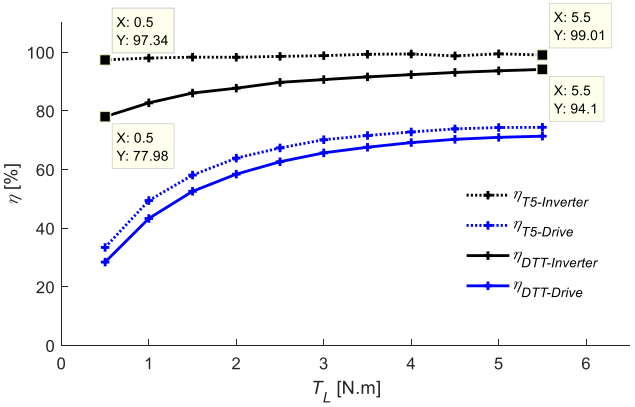

FIGURE 26. Efficiency of the T5MLC drive system compared to DTT drive.

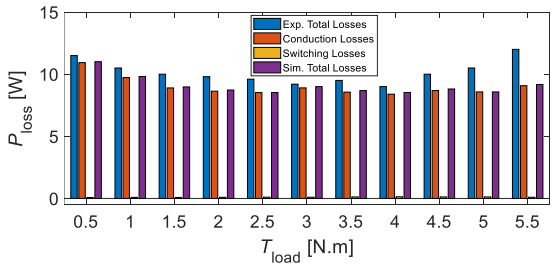

FIGURE 27. Loss breakdown for the T5MLC.

where P_{cond} is the MOSFET conduction loss, I is the RMS value of the drain current, $P_{\text{d-cond}}$ is the diode conduction loss, I_{d} is the RMS value of the diode current and I_{avd} is the mean value of the diode current.

The switching and conduction losses for the proposed T5MLC Loss breakdown for the T5MLC are calculated and compared to the corresponding experimental results in Fig. 27. Slight difference could be observed between simulation and experimental results due to the data acquisition and sensors accuracy. It is worth mentioning that the switching losses at are very small due to the use of SiC MOSFET that has very low turning on and off energies ($E_{on} = 0.5\ mJ$ and $E_{off} = 0.07\ mJ$ at 800 V and 20 A reference values). In addition, it is observed that the T5MLC average switching frequency, using the implemented MPC approach, is 6.87 kHz, which keep the switching losses very small.

TABLE 3. Motor parameters.

MOTOR PARAMETERS

Parameter	Value	Parameter	Value
P_r	1 kW	T_{rated}	5.5 N.m
V_{rated} (ph)	220 V	$\|\|\psi_s\|\|_{rated}$	0.8157 Wb
I_{rated}	2.2 A	R_r	6.0373 Ω
N_{rated}	1710 rpm	L_r	0.4577 H
R_s	8.15 Ω	n_p	2
L_s	0.4577 H	J	0.007 kg.m^2
L_m	0.4372 H	B	0.004 N.s/rad

VII. CONCLUSION

This paper evaluates and implement a SiC-based T5MLC drive system. A mathematical modeling for the T5MLC is discussed. The design considerations for the SiC-based T5MLC are presented and discussed. The converter is tested within a complete IM AC drive system. The drive system is controlled using MPC that controls the machine torque and flux and balance the DC link capacitor voltages. The experimental results are recorded for three different scenarios to evaluate the converter and connected machine performance. The results reflected that the implemented prototype is capable to operate the AC drive system with low torque and flux ripples. In addition, the MPC could balance the DC link capacitor voltages at different scenarios. In addition, the harmonic analysis is performed and reflected reasonable *THD* values for voltage and currents. Moreover, the drive system loss analysis is made to reflect how the drive system is efficient. The results show that the implemented T5MLC efficiency is substantially higher than that of corresponding DTT-MLC.

APPENDIX

See Table 3.

REFERENCES

[1] M. Norambuena, S. Kouro, S. Dieckerhoff, and J. Rodriguez, "Reduced multilevel converter: A novel multilevel converter with a reduced number of active switches," *IEEE Trans. Ind. Electron.*, vol. 65, no. 5, pp. 3636–3645, May 2018.

[2] M. Schweizer and J. W. Kolar, "Design and implementation of a highly efficient three-level T-Type converter for low-voltage applications," *IEEE Trans. Power Electron.*, vol. 28, no. 2, pp. 899–907, Feb. 2013.

[3] A. Salem, F. De Belie, A. Darba, M. Eissa, S. M. Wasfy, and J. Melkebeek, "Evaluation of a dual-T-type converter supplying an open-end winding induction machine," in *Proc. IECON - 39th Annu. Conf. IEEE Ind. Electron. Soc.*, Nov. 2013, pp. 749–754.

[4] M. D. Siddique, S. Mekhilef, N. M. Shah, A. Sarwar, A. Iqbal, and M. A. Memon, "A new multilevel inverter topology with reduce switch count," *IEEE Access*, vol. 7, pp. 58584–58594, 2019.

[5] M. D. Siddique, S. Mekhilef, N. M. Shah, and M. A. Memon, "Optimal design of a new cascaded multilevel inverter topology with reduced switch count," *IEEE Access*, vol. 7, pp. 24498–24510, 2019.

[6] M. D. Siddique, S. Mekhilef, N. M. Shah, A. Sarwar, A. Iqbal, M. Tayyab, and M. K. Ansari, "Low switching frequency based asymmetrical multilevel inverter topology with reduced switch count," *IEEE Access*, vol. 7, pp. 86374–86383, 2019.

[7] M. D. Siddique, S. Mekhilef, N. M. Shah, J. S. M. Ali, M. Meraj, A. Iqbal, and M. A. Al-Hitmi, "A new single phase single switched-capacitor based nine-level boost inverter topology with reduced switch count and voltage stress," *IEEE Access*, vol. 7, pp. 174178–174188, 2019.

[8] A. Salem, M. F. Elsied, J. Druant, F. De Belie, A. Oukaour, H. Gualous, and J. Melkebeek, "An advanced multilevel converter topology with reduced switching elements," in *Proc. IECON 40th Annu. Conf. IEEE Ind. Electron. Soc.*, Oct. 2014, pp. 1201–1207.

[9] M. Elsied, A. Salem, A. Oukaour, H. Gualous, H. Chaoui, F. T. Youssef, D. Belie, J. Melkebeek, and O. Mohammed, "Efficient power-electronic converters for electric vehicle applications," in *Proc. IEEE Vehicle Power Propuls. Conf. (VPPC)*, Oct. 2015, pp. 978–983.
[10] A. Salem and M. A. Abido, "T-type multilevel converter topologies: A comprehensive review," *Arabian J. Sci. Eng.*, vol. 44, no. 3, pp. 1713–1735, Mar. 2019.
[11] J. Kim, D. Shin, and S.-K. Sul, "A damping scheme for switching ringing of full SiC MOSFET by air core PCB circuit," *IEEE Trans. Power Electron.*, vol. 33, no. 6, pp. 4605–4615, Jun. 2018.
[12] J. Biela, M. Schweizer, S. Waffler, and J. W. Kolar, "SiC versus Si—Evaluation of potentials for performance improvement of inverter and DC–DC converter systems by SiC power semiconductors," *IEEE Trans. Ind. Electron.*, vol. 58, no. 7, pp. 2872–2882, Jul. 2011.
[13] I. Roasto, D. Vinnikov, and M. Klytta, "EMC considerations on PCB design for a high-power converter control system," in *Proc. Compat. Power Electron.*, May 2007, pp. 1–4.
[14] A. Corsaro, C. Parisi, and C. Rotay, "EMC design guides for motor control applications," *ST Microelectron.*, 2015. [Online]. Available: https://www.stmicroelectronics.com.cn/content/ccc/resource/technical/document/application_note/f7/f4/51/8d/a1/c5/47/8e/DM00182773.pdf/files/DM00182773.pdf/jcr:content/translations/en.DM00182773.pdf
[15] M. Beye, M. Elsied, A. M. Mabwe, and C. Onambele, "Grid interconnection of renewable energy sources based on advanced multi-level inverter," in *Proc. IEEE Int. Conf. Environ. Electr. Eng. IEEE Ind. Commercial Power Syst. Eur. (EEEIC /I&CPS Europe)*, Jun. 2017, pp. 1–6.
[16] M. Sharifzadeh, H. Vahedi, A. Sheikholeslami, P.-A. Labbe, and K. Al-Haddad, "Hybrid SHM–SHE modulation technique for a four-leg NPC inverter with DC capacitor self-voltage balancing," *IEEE Trans. Ind. Electron.*, vol. 62, no. 8, pp. 4890–4899, Aug. 2015.
[17] K. Wang, Z. Zheng, L. Xu, and Y. Li, "A four-level hybrid-clamped converter with natural capacitor voltage balancing ability," *IEEE Trans. Power Electron.*, vol. 29, no. 3, pp. 1152–1162, Mar. 2014.
[18] J. Zhang, S. Xu, X. Hu, and Y. Zhu, "Voltage balancing control of hybrid stacked multicell converters based on modified phase-shifted PWM," *IEEE Access*, vol. 7, pp. 25589–25602, 2019.
[19] J. Zhang, J. Liu, J. Liu, W. Fang, J. Hou, and Y. Dong, "Modified capacitor voltage balancing sorting algorithm for modular multilevel converter," *J. Eng.*, vol. 2019, no. 16, pp. 3315–3319, Mar. 2019.
[20] U.-M. Choi, J.-S. Lee, and K.-B. Lee, "New modulation strategy to balance the neutral-point voltage for three-level neutral-clamped inverter systems," *IEEE Trans. Energy Convers.*, vol. 29, no. 1, pp. 91–100, Mar. 2014.
[21] U.-M. Choi, F. Blaabjerg, and K.-B. Lee, "Method to minimize the low-frequency neutral-point voltage oscillations with time-offset injection for Neutral-Point-Clamped inverters," *IEEE Trans. Ind. Appl.*, vol. 51, no. 2, pp. 1678–1691, Mar. 2015.
[22] A. Salem, F. De Belie, T. Youssef, J. Melkebeek, O. A. Mohamed, and M. A. Abido, "DC link capacitor voltage balancing of a dual three-level T-type AC drive using switching state redundancy," in *Proc. IEEE Int. Electr. Mach. Drives Conf. (IEMDC)*, May 2017, pp. 1–8.
[23] F. Wang, X. Mei, J. Rodriguez, and R. Kennel, "Model predictive control for electrical drive systems-an overview," *CES Trans. Elect. Mach. Syst.*, vol. 1, no. 3, pp. 219–230, Sep. 2017.
[24] S. Vazquez, J. Rodriguez, M. Rivera, L. G. Franquelo, and M. Norambuena, "Model predictive control for power converters and drives: Advances and trends," *IEEE Trans. Ind. Electron.*, vol. 64, no. 2, pp. 935–947, Feb. 2017.
[25] S. Vazquez, J. I. Leon, L. G. Franquelo, J. Rodriguez, H. A. Young, A. Marquez, and P. Zanchetta, "Model predictive control: A review of its applications in power electronics," *IEEE Ind. Electron. Mag.*, vol. 8, no. 1, pp. 16–31, Mar. 2014.
[26] J. Rodriguez and P. Cortes, *Predictive Control of Power Converters and Electrical Drives*, Vol. 40. Hoboken, NJ, USA: Wiley, 2012.
[27] P. Q. Dzung, N. D. Tuyen, N. T. Tien, and N. C. Viet, "Model predictive current control for T-type NPC inverter using new on-line inductance estimation method," in *Proc. IEEE Region Conf. (TENCON)*, Nov. 2016, pp. 316–321.
[28] J. D. Barros, J. F. A. Silva, and E. G. A. Jesus, "Fast-predictive optimal control of NPC multilevel converters," *IEEE Trans. Ind. Electron.*, vol. 60, no. 2, pp. 619–627, Feb. 2013.
[29] A. S. M. Salem, "Design and analysis of five-level T-type power converters for rotating field drives," Ph.D. dissertation, Ghent Univ., Gent, Belgium, 2015.
[30] D. G. Holmes and T. A. Lipo, *Pulse Width Modulation for Power Converters: Principles and Practice*. Hoboken, NJ, USA: Wiley, Oct. 2003.
[31] A. Salem, M. Mamdouh, and M. A. Abido, "Predictive torque control and capacitor balancing of a SiC-based dual T-Type drive system," *IEEE Trans. Power Electron.*, vol. 35, no. 3, pp. 2871–2881, Mar. 2020.
[32] P. R. U. Guazzelli, W. C. de Andrade Pereira, C. M. R. de Oliveira, A. G. de Castro, and M. L. de Aguiar, "Weighting factors optimization of predictive torque control of induction motor by multiobjective genetic algorithm," *IEEE Trans. Power Electron.*, vol. 34, no. 7, pp. 6628–6638, Jul. 2019.
[33] C. A. Rojas, J. Rodriguez, F. Villarroel, J. Espinoza, and D. A. Khaburi, "Multiobjective fuzzy predictive torque control of an induction motor drive," in *Proc. 6th Power Electron., Drive Syst. Technol. Conf. (PEDSTC)*, Feb. 2015, pp. 3–4.
[34] V. Yaramasu, B. Wu, and J. Chen, "Model-predictive control of grid-tied four-level diode-clamped inverters for high-power wind energy conversion systems," *IEEE Trans. Power Electron.*, vol. 29, no. 6, pp. 2861–2873, Jun. 2014.
[35] "Renewable energy solutions: Energy efficient components for PV solar systems," Fair-Child Appl. Note, 2012. [Online]. Available: https://docplayer.net/13332454-Renewable-energy-solutions-energy-efficient-components-for-pv-solar-systems.html
[36] C. Hayes. *Using SiC Devices in a Three-Phase Motor Drive Application*. Application Note, Accessed: Jul. 18, 2015. Available at. [Online]. Available: https://www.electronicspecifier.com/products/power/using-sic-devices -in-a-three-phase-motor-drive-application
[37] P. Cortes, S. Kouro, B. La Rocca, R. Vargas, J. Rodriguez, J. I. Leon, S. Vazquez, and L. G. Franquelo, "Guidelines for weighting factors design in model predictive control of power converters and drives," in *Proc. IEEE Int. Conf. Ind. Technol.*, Feb. 2009, pp. 1–7.
[38] M. H. Bierhoff and F. W. Fuchs, "Semiconductor losses in voltage source and current source IGBT converters based on analytical derivation," in *Proc. IEEE 35th Annu. Power Electron. Spec. Conf.*, Jun. 2004, pp. 2836–2842.

ABOUBAKR SALEM (Member, IEEE) received the B.Sc. and M.Sc. degrees in electrical engineering from Helwan University, Egypt, in 2004 and 2009, respectively, and the Ph.D. degree from Ghent University, Belgium, in 2015. He is currently a Visiting Assistant Professor with the Electrical Engineering Department, King Fahd University of Petroleum and Minerals (KFUPM). He is involved in several funded projects from KFUPM as a Pi and Co-I. He has participated as a Co-I in funded projects from the European Union (i.e., STS-Med and Euro-Sun-Med) with a fund of AC 20 million. His research interests include power electronic converters design and control, electrical drives applications, renewable energy integration, electrical vehicles, and smart grid applications.